# Diamagnetic thresholds for sawtooth cycling in tokamak plasmas

Federico D. Halpern, Hinrich Lütjens, and Jean-François Luciani

Citation: Phys. Plasmas **18**, 102501 (2011); doi: 10.1063/1.3646305
View online: http://dx.doi.org/10.1063/1.3646305
View Table of Contents: http://pop.aip.org/resource/1/PHPAEN/v18/i10
Published by the American Institute of Physics.

# Diamagnetic thresholds for sawtooth cycling in tokamak plasmas

Federico D. Halpern,[a] Hinrich Lütjens, and Jean-François Luciani
*Centre de Physique Théorique, École Polytechnique, CNRS, 91120 Palaiseau, France*

(Received 1 June 2011; accepted 2 September 2011; published online 10 October 2011)

The cycling dynamics of the internal kink mode, which drives sawtooth oscillations in tokamak plasmas, is studied using the three dimensional, non-linear magnetohydrodynamic (MHD) code XTOR-2F [H. Lütjens and J.-F. Luciani, J. Comput. Phys. **229**, 8130 (2010)]. It is found that sawtooth cycling, which is characterized by quiescent ramps and fast crashes in the experiment, can be recovered in two-fluid MHD provided that a criterion of diamagnetic stabilization is fulfilled. The simulation results indicate that diamagnetic effects alone may be sufficient to drive sawteeth with complete magnetic reconnection in high temperature Ohmic plasmas. © *2011 American Institute of Physics*. [doi:10.1063/1.3646305]

## I. INTRODUCTION

Sawtooth relaxations are characterized by a magnetic reconnection event with $q=m/n=1/1$ helicity that periodically redistributes heat, current, and particles in the plasma core of magnetically confined devices.[1,2] These magnetic relaxation events (crashes) are separated by quasi-quiescent periods of time (ramps) during which the plasma pressure within the resonant surface increases and the mode is believed to be stable. Precursor and postcursor oscillations often precede and succeed sawtooth crashes in tokamaks.

In the present tokamak experiments, sawtooth crashes are widely believed to provide the finite amplitude perturbation necessary to seed neoclassical tearing modes. In future devices, where the population of fast ions will be large, sawteeth may have a large effect on the fast particle confinement through coupling or triggering of kinetic instabilities (see, for example, Refs. 3–5). Although increased understanding of sawtooth oscillations would be important for successful tokamak operation, the sawtooth cycle is not completely resolved. The present work is concerned with the dynamics of kink cycling, i.e., with the conditions that allow the repetitive succession of ramps, precursor, crash, and postcursor stages, that is observed in tokamak experiments during each sawtooth cycle.

The analytical theory has identified asymptotic regimes for the $m/n=1/1$ internal kink mode and described their dynamics.[6–14] It is noted that in ideal magnetohydrodynamics (MHD), with no dissipation mechanism available to enable magnetic reconnection, an unstable kink mode results in a three dimensional equilibrium with a $m/n=1/1$ helicity component (no kink cycles). In resistive MHD, kink cycles can be recovered, but the duration of kink crashes, $\tau_{\mathrm{crash}}\sim\eta^{-1/2}$, is several orders of magnitude too slow with respect to the sawtooth crashes observed in large tokamaks.[15–17] When diamagnetic flows are included in the description of the internal kink, the growth rate of the resistive instability is further reduced and the mode can become completely stable.[8,13]

It is also noted that the ideal MHD time scale required to recover the short crash times observed in the experiment appears to be at odds with the slow growth rate (in the resistive time scale) of the precursor oscillations that precede the crash. Several authors have proposed models that involve an acceleration of the reconnection rate during the late stage of the sawtooth ramp.[12,18–22]

In a preceding work,[23] the internal kink dynamics were studied, revealing a threshold between cases displaying a saturated $m/n=1/1$ helical state in the plasma core, and regimes where the kink is oscillating in time. The transition between these dynamics is controlled by plasma pressure, resistivity, thermal transport, and diamagnetic effects. It was shown with 3D extended MHD simulations that sawtooth cycles with physical parameters typical of Ohmic tokamak plasmas can be observed only in the framework of resistive MHD with thermal transport and diamagnetic effects. Without the latter effect, the kink dynamics only displays saturated stationary helical states or oscillatory regimes with comparable ramp and crash times.

In the present work, we investigate quantitatively how the interplay between resistivity and diamagnetic flows affects the *shape* of the kink cycle by means of non-linear 3-D two-fluid MHD simulations. Two diamagnetic thresholds between three different cyclic regimes are found, and criteria for the critical diamagnetic stabilizations at the regime transitions are obtained. Our study starts with an equilibrium that, in resistive MHD with transport, evolves nonlinearly into a $m/n=1/1$ helical state due to a low-shear pressure driven instability[9,10] (no kink cycles). Above a threshold of diamagnetic stabilization, we observe resistive internal kink cycles more or less following Kadomtsev's predictions,[7] for instance, as discussed in Refs. 15–17. Above a second threshold of diamagnetic stabilization, we find a regime of kink cycles characterized by quiescent ramps, slow-growing precursors, and fast crashes.

Following the determination of the diamagnetic thresholds for the sawtooth-like regime, it is hypothesized that the ramp and crash dynamics of the internal kink in plasmas with Lundquist number $S\geq 10^7$–$10^9$ are always dominated

[a]Present address: École Polytechnique Fdrale de Lausanne (EPFL), Centre de Recherches en Physique des Plasmas, Association Euratom-Confdration Suisse, CH-1015 Lausanne, Switzerland. Electronic mail: federico.halpern@epfl.ch.

 

by the diamagnetic rotations and that their cycle dynamics resemble experimental observations even in a two-fluid MHD description.

The physical model used to carry out the study is briefly described below in Sec. II. Then, the simulation results are described in Sec. III. In particular, the characteristic of the different kink cycle dynamics is discussed in Sec. III B; a discussion regarding the diamagnetic thresholds between these different regimes is found in Sec. III C; In Sec. IV, details of the dynamics of the pressure in these different regimes are discussed. The conclusions of the study are presented in Sec. V.

## II. PHYSICAL MODEL

The physical model used to study the ramp dynamics of the internal kink mode is briefly summarized here. The simulations are carried out with the XTOR-2F code.[24] The physical model is fully toroidal and non-linear; and it includes resistivity, viscosity, diamagnetic drifts, and anisotropic thermal transport. This system results from Braginskii's two-fluid model,[25] with the approximation $\mathbf{v}_i = (\mathbf{E}\times\mathbf{B})/B^2 + \mathbf{v}_{*i}$,

$$\partial_t \rho = -\rho\nabla\cdot\mathbf{v} - \mathbf{v}\cdot\nabla\rho - \alpha\nabla p_i\cdot\nabla\times\mathbf{B}/B^2 + \nabla\cdot D_\perp\nabla(\rho-\rho_{t=0}), \quad (1)$$

$$\rho\partial_t\mathbf{v} = -\rho(\mathbf{v}\cdot\nabla)\mathbf{v} - \rho(\mathbf{v}_{*i}\cdot\nabla)\mathbf{v}_\perp + \mathbf{J}\times\mathbf{B} - \nabla p + \nu\nabla^2\mathbf{v}, \quad (2)$$

$$\partial_t p = \Gamma p\nabla\cdot\mathbf{v} - \mathbf{v}\cdot\nabla p - \alpha\Gamma\frac{p}{\rho}\nabla p_i\cdot\nabla\times\mathbf{B}/B^2 + \nabla\cdot\chi_\perp\nabla_\perp(p-p_{t=0}) + \nabla\cdot\chi_\parallel\nabla_\parallel p, \quad (3)$$

$$\partial_t\mathbf{B} = \nabla\times(\mathbf{v}\times\mathbf{B}) + \alpha\nabla\times\nabla_\parallel p_e/\rho - \nabla\times\eta\mathbf{J}. \quad (4)$$

Here, the velocity evolved is $\mathbf{v} = \mathbf{E}\times\mathbf{B}/B^2$, while the diamagnetic velocities are computed as needed in the computation. The collisional Braginskii heat flux is not retained, and the transport model is restricted to $\chi_\perp$ and $\chi_{||}$. The collisionless Braginskii cross-field heat flux is combined with the $\mathbf{v}_{*i}$ convection, resulting in Eq. (3). The simplest form of the gyroviscous stress tensor is adopted, which results in the simplification $d_t\mathbf{v}_* + \nabla\cdot\mathbf{\Pi}_\mathbf{g} \approx \nabla p$, while the momentum equation is similar to the equation derived in Ref. 26.

The diamagnetic flow terms scale like the ion skin depth $\alpha = (\omega_{ci}\tau_a)^{-1} = (c/(a\omega_{pi}))$ (here, $\omega_{ci} = ZeB_u/m_i$ is the ion cyclotron frequency, $\tau_a = (\mu_0\rho_0)^{1/2}a/B_u$ is the Alfvén time, $\omega_{pi} = (m_i\epsilon_0/(Z^2e^2n_i))^{1/2}$ is the ion plasma frequency, and $B_u = aB_0/R_0$ is the unit magnetic field). The ion diamagnetic velocity is given by $\mathbf{v}_{*i} = \alpha\mathbf{B}\times\nabla p_i/(\rho B^2)$. In the above equations, the initial resistivity profile $\eta$ is evaluated by imposing $\eta J_\Phi = E_\Phi$ to be constant for the initial equilibrium, $\chi_\perp = \chi_{\perp 0}\eta/\eta_0$ and $\chi_{||}$ are the thermal diffusivity coefficients (the index 0 indicates the value at the axis). $D_\perp = \chi_\perp/10$ is the particle diffusivity, $\nu = 5.0\times10^{-6}$ is the viscosity, and $\Gamma = 5/3$ is the ratio of specific heats. In the simulations, these quantities are all constant in time.

Equations (1) and (3) include source terms (through the perpendicular diffusion operators) which restore the pressure and density profiles within their characteristic diffusion times. It is emphasized that the evolution of the "equilibrium profiles" is driven by the initial equilibrium sources and shapes of resistivity and diffusivity in the case of a static $\eta$ profile and diffusivity only in the case of a time evolving $\eta \propto (p(t)/\rho(t))^{-3/2}$, according to Spitzer's law (for the numerical method, see Ref. 27). Therefore, the initial "equilibrium profiles" are never strictly recovered during the cycling dynamics described in the following.

Selected simulations comparing a static $\eta$ and Spitzer $\eta$ have shown that the overall cycling dynamics remains unchanged. Only the thresholds between the different cycling regimes described in Secs. III and IV are relocated to a slightly higher value of the Lundquist number $S = 1/\eta_0$. Indeed, with Spitzer $\eta$, as for the pressure and the current profiles, the initial resistivity profile is never strictly recovered, i.e., $\eta$ in the plasma core remains larger than its initial value during the cycling regime. For example, in a case with initial $\eta_0 = 10^{-7}$ and $\eta_{q=1}/\eta_0 = 1.60$, with Spitzer $\eta$ and $\alpha = 0.1$, $\eta_{q=1}/\eta_0(t) \approx 1.52$ at the end of the ramp phases in the cycling regime. Including Spitzer $\eta$ has, however, an odd numerical side effect on the iterative solver in XTOR-2F[24] because it converges significantly slower at large $\alpha$ than with static $\eta$. Therefore, to maintain the CPU time of our study within reasonable bounds, we decided to use static diffusion and resistivity profiles in the study to follow.

Equal ion and electron pressure are assumed, $p_e = p_i = p/2$. However, we note that due to the large $\chi_{||}$, the effective $\omega_{*e}$ is principally due to the variation of the density, i.e., $\omega_{*e} \approx \omega^n_{*e} = -\alpha\mathbf{B}\times T\nabla\rho/(r_1\rho B^2)$, where $r_1 = r(q=1)$ is the physical radius at the $q=1$ surface. The gradient of the density profile is moderately flat resulting in $\omega^n_{*e} \approx \omega_{*i}/9$ at the $q=1$ surface.

## III. CHARACTERIZATION OF THE INTERNAL KINK CYCLING DYNAMICS

In this section, the results of the non-linear simulations are described. We are interested in studying the thresholds between different non-linear steady state cyclic regimes. In consequence, the simulations must be evolved until the amplitude and frequency of the kink cycles become constant, or until the kink mode reorganizes the magnetic field topology into a stationary equilibrium with $m/n = 1/1$ helicity.

### A. Set up of physical parameters for the simulations

Non-linear internal kink mode simulations are carried out including the toroidal harmonics $n = 0, 1, 2, 3$. For $n = 1, 2, 3$, the harmonics retained have $n-4 \le m \le n+7$. The $n=0$ mode, for which 8 poloidal modes are retained, initially corresponds to the equilibrium fields. The starting equilibrium is computed using the CHEASE code.[28] The equilibrium boundary is circular, with aspect ratio $R_0/a = 2.7$. The pressure and magnetic $q$ profiles used for the study are shown in Fig. 1. The equilibrium has a parabolic $q$ profile with $q_0 = 0.77$, $q_{edge} = 5.4$, $\hat{s}_{q=1} = 0.4$ ($\hat{s} = (s/q)(dq/ds)$ is the magnetic shear, with $s = (\psi/\psi_s)^{1/2}$ and $\psi$ the equilibrium poloidal magnetic flux). The radial profile of poloidal beta, $\beta_p = 2\mu_0 p/B_\theta^2$, is almost flat. The equilibrium used in the simulations has $\beta_p \approx 0.22$, which is about 2/3 of threshold for the ideal MHD

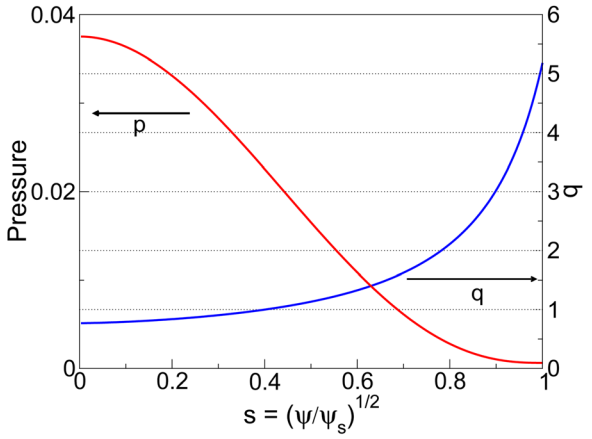


FIG. 1. (Color online) Initial equilibrium pressure and $q$ profiles.

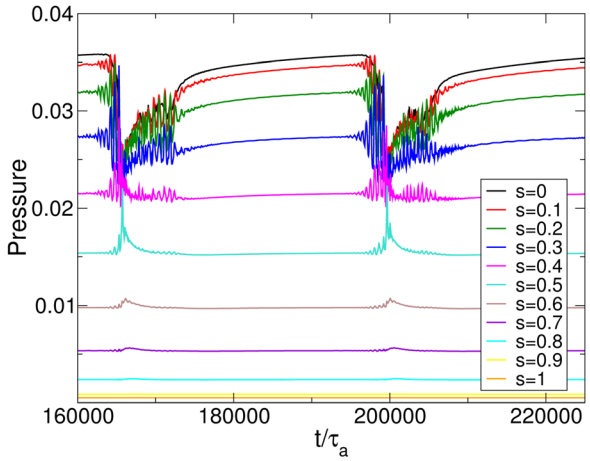


FIG. 2. (Color online) Pressure versus time in XTOR-2F simulation of internal kink cycling with fast crashes, $S=2/3\times10^7$, $\beta_p=0.22$, and $\alpha=0.15$. The radial coordinate of each radial location is given by $s=(\psi/\psi_s)^{1/2}$.

kink ($\beta_{p,thresh}=0.33$). The ideal instability threshold was determined with XTOR-2F simulations of the linear growth phase with $n=0$ and $n=1$.

The kink cycle dynamics are strongly influenced by the resistive diffusion time $\tau_\eta=1/\eta=S$, which affects the growth rate of the internal kink and the relaxation of the $q$ profile after each crash; and the characteristic energy diffusion time $\tau_{\chi\perp}=1/\chi_\perp$, which acts through the source term in Eq. (3). (The characteristic times are given in internal units, $a=1$, $\tau_a=1$, $\mu_0=1$). Simulations are carried out using $\tau_\eta/\tau_{\chi\perp}=\chi_\perp/\eta=30$, while in tokamak experiments $\tau_\eta/\tau_{\chi\perp}\approx100$.

For instance, in a previous study[23] it was found that there is a competition between $\tau_\eta$, $\tau_{\chi\perp}$, and $\beta_p$ through the aforementioned plasma sources. Non-decaying kink cycles could be recovered depending on the ratio of the resistive diffusion time $\tau_\eta=\mu_0a^2/\eta$ to the perpendicular energy diffusion time $\tau_{\chi\perp}=a^2/\chi_\perp$, the poloidal beta, and the diamagnetic stabilization effect (which scales like $\alpha$).

In addition, the time scales in the kink dynamics are modified by the diamagnetic rotations. For example, in the resistivity dominated regime with diamagnetic flows, the linear growth rate of the internal kink at the marginal ideal stability point[8] can be expressed in the form $\gamma(\gamma-i\omega_{*i})(\gamma+i\omega_{*e})\simeq\eta$. Thus, if $S$ is to be varied while maintaining the characteristic timescale of this particular asymptotic regime constant, it is expected that the quantity $S^{-1/3}/\alpha$ should be kept constant. For instance, in the JET tokamak, using $R_0=3.1$ m, $B_0=2.7$ T, $n_0=2.0\times10^{19}$ m$^{-3}$, $T_e=2$ keV, we obtain $\alpha\approx0.08$ and $S\approx2\times10^8$. Keeping $S^{-1/3}/\alpha$ constant, but decreasing the Lundquist number to $S=10^7$ we find $\alpha\approx0.2$. In the present paper, $S=10^6$–$10^7$ and $\alpha=0$–$0.2$. Note, however, that these scalings are different for each asymptotic regime of the internal kink.

Three different cyclic regimes are recovered in the simulations: a regime of helicoidal equilibria characterized by a saturated $m/n=1/1$ flat shear instability[9,10] (no kink cycles); a regime of non-decaying, sustained kink cycles characterized by slow, resistivity-driven crashes;[15–17] and a regime of sustained kink cycles with fast crashes, i.e., a sawtoothing regime. An example of the pressure evolution at different plasma radii for the sawtoothing regime is presented in Fig. 2. Below, the dynamics of the two cycling regimes are analysed. Then, the diamagnetic thresholds separating each cyclic regime are studied.

### B. Differences in the kink dynamics in the two cycling regimes

In this section, we seek to characterize the dynamics in the two regimes where kink cycles take place. In particular, we determine how their timescales are affected by the resistivity and by the diamagnetic effects. One of our objectives is to determine the critical ion skin depth $\alpha_{\rm crit}$ at which the internal kink dynamic transitions between different cyclic regimes occurs.

To that effect, the lengths of each stage of the cycle are estimated in the different regimes. The following criteria is used to determine the length of the precursor, crash, and ramp times: (a) The start of the precursor stage is given by the time of maximum central pressure, when $p_0$ starts deviating from the maximum pressure due to a radial displacement (the maximum pressure, however, is still increasing); (b) the crash starts when the core pressure starts collapsing and the pressure inside the $q=1$ surface starts decreasing; (c) the ramp stage starts when the central pressure reaches a minimum. Fig. 3 shows $p_0$ and the maximum pressure at a line of sight in order to illustrate the criteria. It can be observed that the maximum of pressure is still increasing during the precursor stage.

The ramp, precursor, and crash times for the cases with $S=10^7$ are given in Fig. 4 as a function of the ion skin depth $\alpha$. The lower bound of $\alpha$, i.e., $\alpha_{\rm crit,1}$ in Fig. 4, is given by the critical stabilization required for kink cycles to occur. The duration of the precursor stage always appears to be in the order of 1000–3000$\tau_a$. The crash time increases with increasing $\alpha$ and then abruptly decreases by almost an order of magnitude at the second critical diamagnetic threshold ($\alpha_{\rm crit,2}$ in Fig. 4). Above the second diamagnetic threshold, the crash time is shortened as the diamagnetic stabilization is increased, in qualitative agreement with the crash time dependence computed in Ref. 12. On the other hand, the

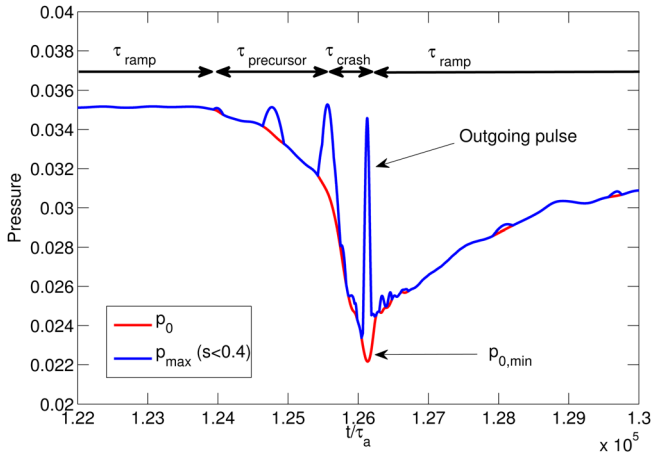


FIG. 3. (Color online) Central pressure and maximum pressure at $\theta=\phi=0$, inside $s=(\psi/\psi_s)^{1/2}<0.4$, are shown to illustrate the different stages of the kink cycles.

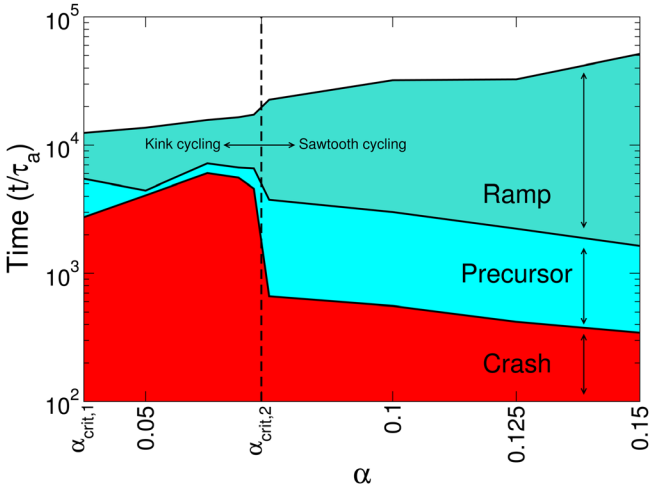


FIG. 4. (Color online) Ramp, precursor, and crash times are shown as a function of the ion skin depth $\alpha$ for cases with $S=10^7$. Shaded area indicates the duration of each stage for a given $\alpha$, while the total cycle time is given by the sum of the duration of the three stages.

lengths of the ramp and kink cycle overall increase by a factor of 3 with the diamagnetic stabilization.

Poloidal cross sections of the magnetic field up to $s=(\psi/\psi_s)^{1/2}\approx 0.5$ for the case in Fig. 2 with $\alpha>\alpha_{\mathrm{crit},2}$ are displayed in Fig. 5 in order to illustrate the topology of the magnetic field during the different stages of a kink cycle. Fig. 5(a) shows the $m/n=1/1$ precursor island. As this precursor grows, it displaces the pressure core toward the $q=1$ surface, and a thin plasma ribbon between the two ends of the island forms. Fig. 5(b) shows the precursor island at the end of the precursor stage. Significant $m=2$ and $m=3$ components and some field stochasticity are observed; an X-point is formed on the left/middle of the pattern, triggering the fast crash phase. This transition from a "Y-line" reconnection to a "X-point" one is generally linked with the acceleration of the reconnection that we observe. During the crash phase, as shown in Fig. 5(c), the poloidal cross section of the displaced hot core adopts an asymmetric tear shape as it rotates around the magnetic axis. Following the crash, the inner 30% of the plasma radius is occupied by remains of the precursor chain in Fig. 5(d), with mixed $n=1$, 2, 3 helicity.

The evolution of the $q$ profile during a sawtooth cycle is diagnosed during the simulations. The magnetic $q$ at the axis, $q_0$, is about 0.9 at the beginning of the precursor stage. The precursor flats out the $q$ profile around the $q=1$ magnetic surface as it grows, but $q_0<1$ before the crash. Following the crash, $q>1$ inside the mixing radius of about 45%, i.e., the reconnection is complete. The postcursor islands are long-lived as can be observed in Fig. 2 and drive a secondary reconnection event that takes place in a slower time scale than the principal crash, and that starts while the $q$ profile is slightly inverted, with $q_{min}\sim 1.01$. Following this "mini-crash," the postcursor damps away and $q_0$ begins to drop. The cycle completes with a quiescent ramp of the pressure during which $q_0$ drops to about 0.9 until a new precursor grows.

### C. Diamagnetic thresholds for internal kink cyclic regimes

In this section, the transition between the different cyclic regimes is discussed in terms of the critical ion skin depth $\alpha$ and the plasma resistivity. The relevant parameter space for each regime is obtained by carrying out simulations including diamagnetic flows at $\beta_p=0.22$, $\tau_\eta/\tau_{\chi\perp}=30$, $D_\perp=\chi_{||}/10$, and $\chi_{||}/\chi_\perp\approx 10^7$. Simulations are performed by varying $\alpha=0-0.2$ and $S=10^6$–$10^7$.

Two different regime transitions triggered by the diamagnetic stabilizations are found. In resistive MHD with heat and particle diffusion ($\eta\chi$MHD), the non-linear steady state regime found is an equilibrium state with $m/n=1/1$ helicity due to a pressure driven, low shear instability.[9,10] At the first regime transition, the diamagnetic stabilization gives rise to a regime of sustained kink cycles. The dynamics observed in this regime are similar to kink cycling in resistive MHD,[15–17] with collision driven crashes roughly following Kadomtsev's prediction.

A second regime transition occurs if the internal kink is strongly stabilized by the diamagnetic flows. In this cyclic regime, it is observed that the ramp is quiescent and that the dynamics of the crash are strongly modified by diamagnetic effects.[12,20,21,29]

The pattern of cyclic regimes obtained using the two-fluid model (Eqs. (1)–(4)) as a function of $S=1/\eta$ and $\alpha=(\omega_{ci}\tau_a)^{-1}$ is shown in Fig. 6. The triangles represent sawtooth cycling with fast crashes, the circles represent sustained "classical" kink cycles with Kadomtsev-like resistive crashes, and the squares represent stationary equilibria with $m/n=1/1$ helicity due to a saturated kink. Note that the last column of points at $S=10^7$ in Fig. 6 corresponds to the cases shown in Fig. 4.

Non-linear regression fits computed at the thresholds are shown in Fig. 6. A fit of the first transition boundary has the form $\alpha_{\mathrm{crit}}=\alpha_1 S^{-0.34}\approx\alpha_1 S^{-1/3}$; while the transition to the sawtoothing regime has the form $\alpha_{\mathrm{crit}}=\alpha_2 S^{-0.60}=\alpha_2 S^{-3/5}$. The threshold values of $\alpha$ were obtained using the bisection method at fixed $S$ to a precision of the order $\epsilon_\alpha\approx 0.005$.

Estimates of kink cycle stability are often presented in $\omega_*/\gamma_\eta$ versus $\lambda_H/\gamma_\eta$ space.[13] Fig. 7 shows such a diagram for a sequence of instability obtained with our simulations ($\gamma_\eta$ is the growth rate of the resistive kink mode, while

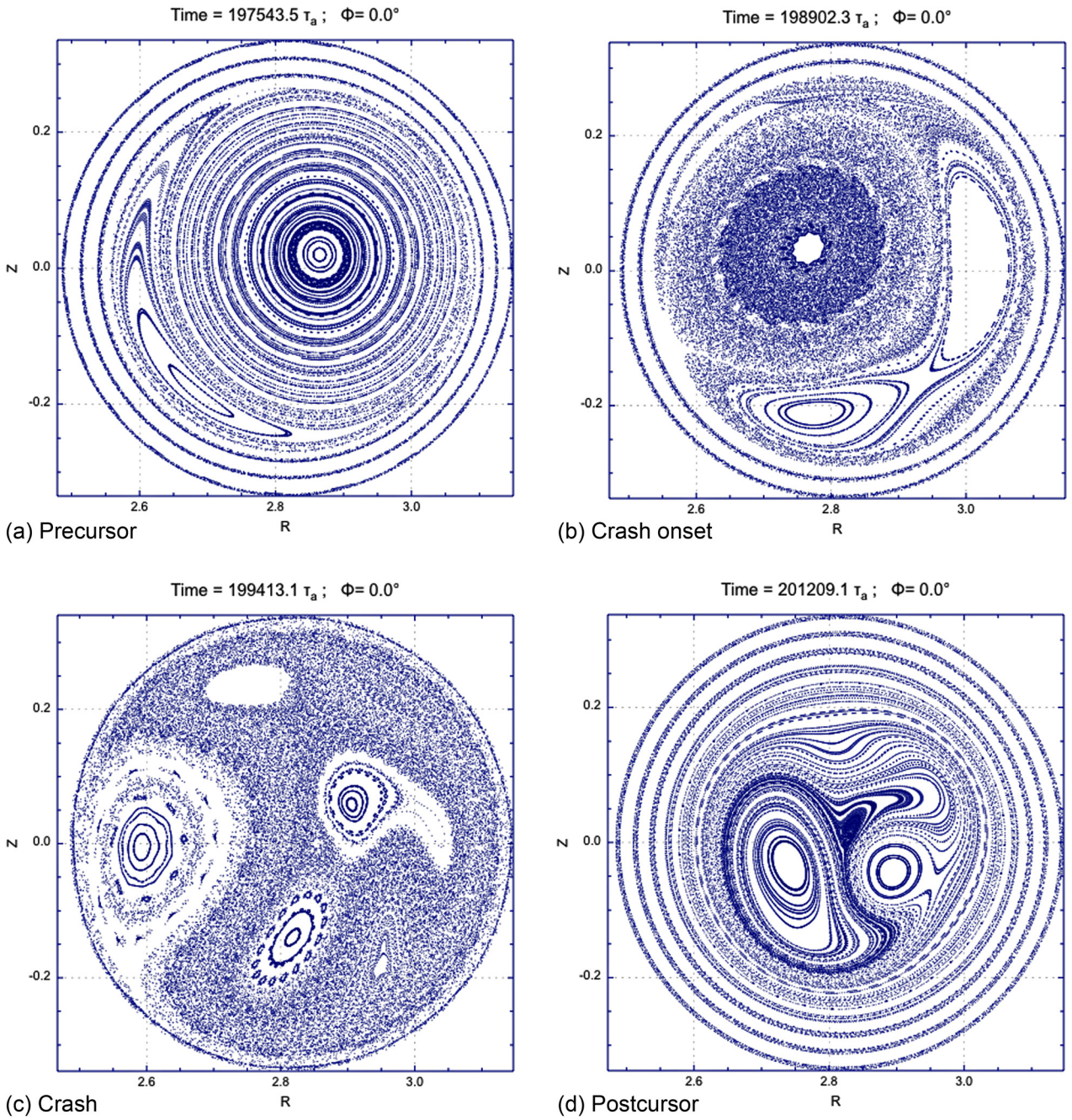


FIG. 5. (Color online) Cross sections of the magnetic field at the (a) precursor precursor, (b) onset onset, (c) crash crash, and (d) postcursor postcursor stages during the sawtooth cycle are shown in Fig. 2. The plots show surfaces with $s=(\psi/\psi_s)^{1/2}<0.5$.

$\lambda_H \sim r_1^2/R^2(\beta_p^2-\beta_{p,\mathrm{crit}}^2)$ is the normalized energy of the internal kink mode[6] or its growth rate when $\lambda_H>0$). The value of $\omega_*$ at the resonant surface $q=1$ was obtained from our simulations; the growth rate $\gamma_\eta$ was obtained from XTOR-2F simulations starting from the relaxed profiles at the ramp and precursor stages and switching off nonresistive MHD terms. Using ideal MHD simulations of the relaxed profiles to estimate the critical poloidal beta $\beta_{p,\mathrm{crit}}$, the formula in Appendix B in Ref. 14 yields $\lambda_H=-1.5\times10^{-3}$. This result is confirmed by extrapolating the linear growth rate found for the ideal kink into the stable region using a fit of the form $\lambda_H \propto (\beta_p^2-\beta_{p,\mathrm{crit}}^2)$.

The figure includes a case with resistive kink cycles (circles) and two cases with sawtooth cycles (diamonds and triangles). All cases have $\alpha=0.1$ and the points shown are during the ramp and at the onset of the precursor oscillations. The case with $S=6.66\times10^6$ is just above the second diamagnetic threshold. This figure can be qualitatively compared, for instance, with the stability diagram shown in Fig. 1 of Ref. 13. It can be observed that the transition between "kink cycling" and "sawtooth cycling" corresponds fairly well with the stability boundary in the diagram presented by Migliuolo,[13] provided that the case with small $\omega_{*e}/\omega_{*i}$ is retained.

The resistive kink cycles have $\lambda_H/\gamma_\eta$ close to $-1$ during the ramp ($\gamma\sim S^{-3/5}$), and their trajectory in stability space moves toward marginal ideal stability as the crash approaches. On the other hand, the sawtoothing cases observed correspond to a regime with more negative $\lambda_H/\gamma_\eta$.

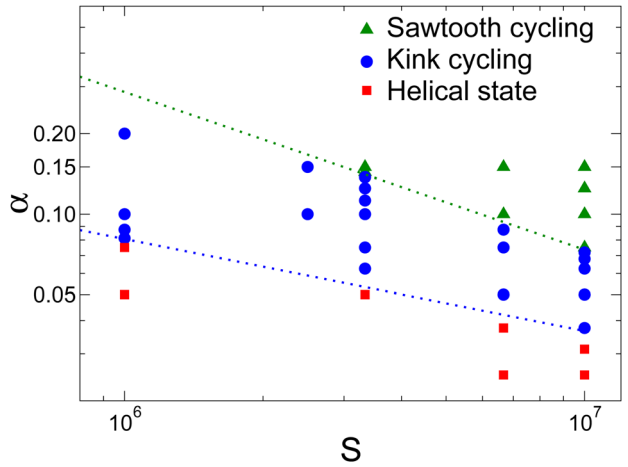


FIG. 6. (Color online) Cyclic regimes found as a function of $\alpha = (\omega_{ci}\tau_a)^{-1}$ and $S = 1/\eta$.

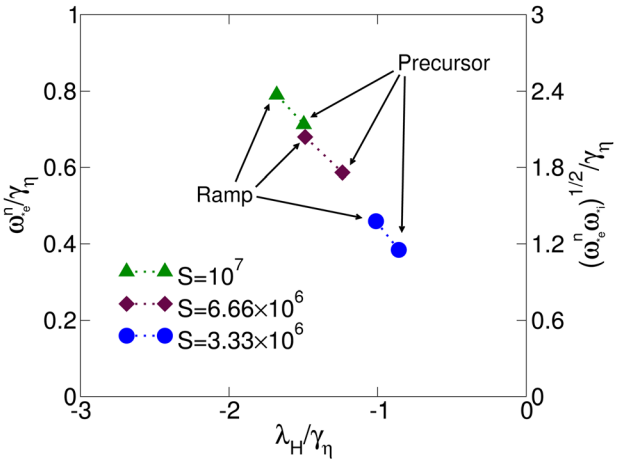


FIG. 7. (Color online) Estimates of trajectories in $\omega_*/\gamma_\eta$ vs $\lambda_H/\gamma_\eta$ stability space are shown for a resistive kink cycle (circles) and two cases with sawtooth cycles (diamonds and triangles). The case with $S = 6.66 \times 10^6$ is just above the diamagnetic threshold for sawtooth cycling. All cases have $\alpha = 0.10$.

During the ramp, the internal kink appears to be stabilized by the diamagnetic effects. The precursor oscillations would correspond to a tearing-like mode destabilized by the pressure drive, followed then by a transition to fast reconnection driven by diamagnetic effects.

The physical effect responsible for the transition between the $m/n = 1/1$ helical state and kink cycling has been described as a competition between the relaxation of the $q$ profile after each crash, the sources that rebuild the pressure core, and the diamagnetic stabilization.[23] In Sec. IV, we examine the characteristic properties of the kink cycles in order to clarify the physical mechanisms that give rise to the second regime transition.

## IV. DETAILS IN PRESSURE PROFILE DYNAMICS OF CYCLING REGIMES

In the subsections below, the ramp dynamics in the resistive cycling and in the sawtoothing regimes are examined. Additionally, a case very close to the second diamagnetic threshold, $\alpha_{crit} = \alpha_2 S^{-3/5}$, is studied. When the periods and amplitudes of the pressure cycles obtained in the simulations are compared, several trends arise. The amplitude of the pressure relaxations observed in the sawtooth regime is between 30% and 45%; while the amplitude of the pressure relaxations observed in the sustained kink cycling regime is generally in the order of 25%. The cycle periods increase with increasing $S$ or $\alpha$. However, no clear scaling emerges, for instance, at the stabilization thresholds where the scaling of the plasma dynamics respect to the dimensionless variables are most likely to remain unchanged. The pressure dynamics in each regime are described below.

### A. Resistive kink cycling regime

The pressure profile relaxation timescale in the resistive cycling regime with $\alpha_1 S^{-1/3} < \alpha < \alpha_2 S^{-3/5}$ (circles in Figs. 6 and 7) are compared using different resistivity values. We concentrate within a short time window around $t_0$, the time of lowest central pressure during a kink cycle. Fig. 8(a) shows the central pressure as a function of time for four different simulations. For the cases shown, the Lundquist number is varied between $S = 10^6$ and $S = 10^7$, and diamagnetic drifts are included. Here, we concentrate on the effect of the resistivity, while the effect of the diamagnetic drifts is shown in Fig. 4. Clearly, the profile relaxation time scales are

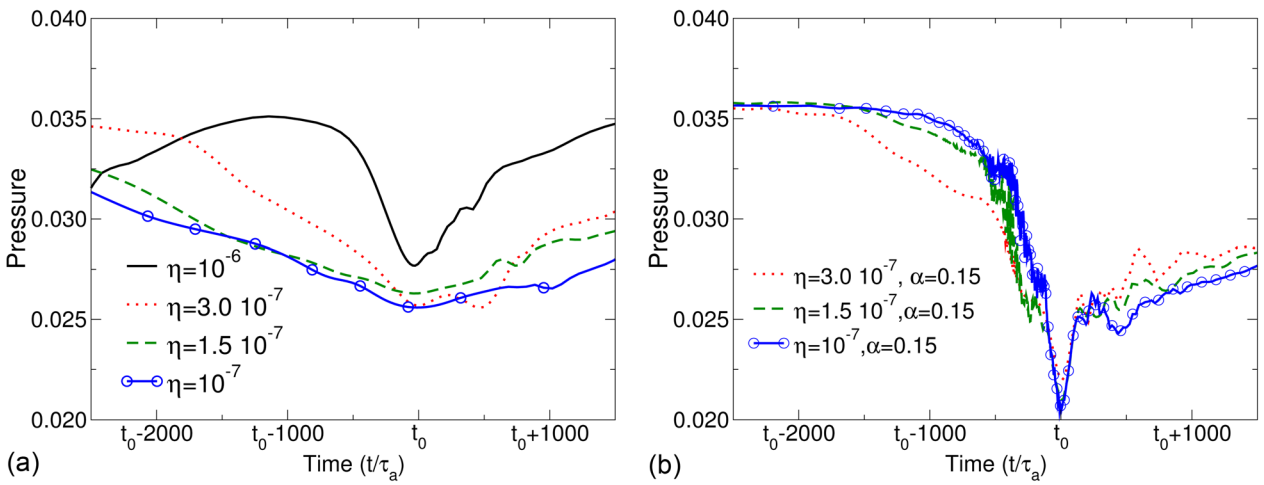


FIG. 8. (Color online) Central pressure versus time is shown for internal kink cases with (a) slow, resistive crashes or (b) diamagnetic fast crashes.

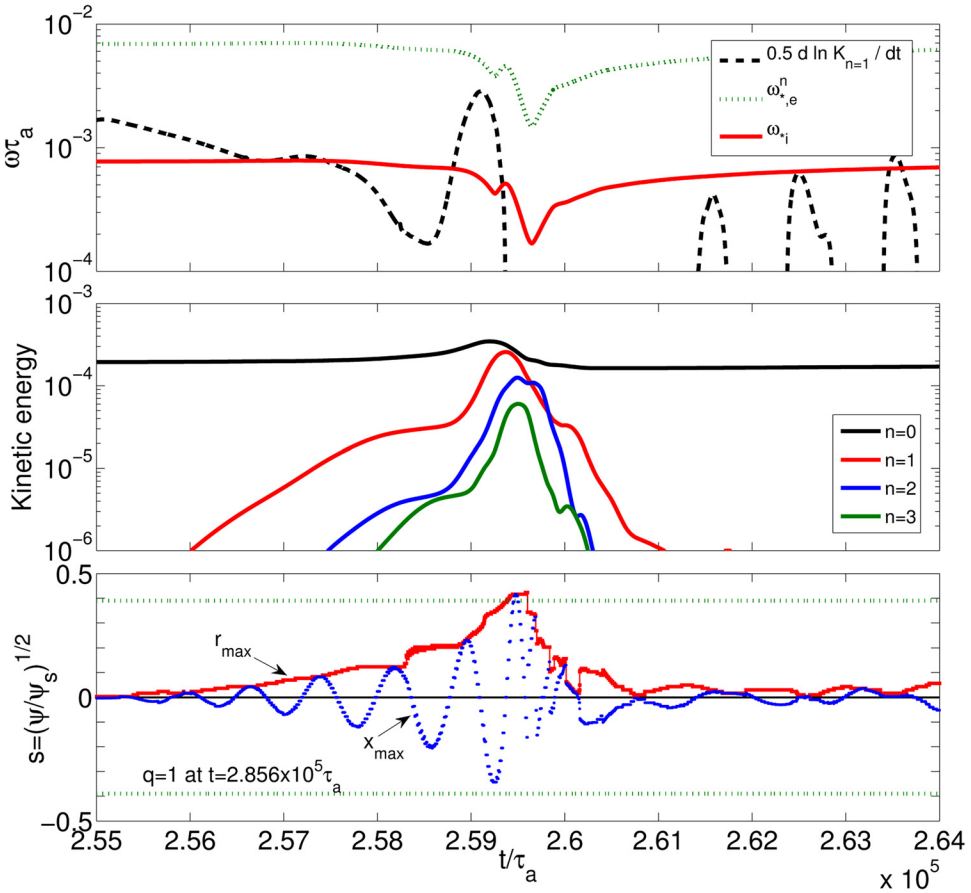


FIG. 9. (Color online) Top: rate of change of the kinetic energy of the $n=1$ mode $\left(\frac{1}{2}\frac{d}{dt}\ln K_{n=1}\right)$ and diamagnetic frequencies at $q=1(\omega_{*i},\omega^n_{*e})$ (note that $\frac{1}{2}\frac{d}{dt}\ln K_{n=1}$ has units of frequency $\omega\tau_a$). Center: zoom on kinetic energies $K_{n=0,1,2,3}$ in the vicinity of the crash, showing an abrupt change in the instability time scale. Bottom: Radius ($r_{peak}$) and horizontal position ($x_{peak}$) of the peak pressure at the $\phi=\theta=0$ line of sight. Position is measured using $s=(\psi/\psi_s)^{1/2}$. In this simulation, $S=10^7$, $\alpha=0.10$.

lengthened as the resistivity is decreased. The evolution of the central pressure during the crash denotes resistive internal kink behaviour, i.e., the duration of the pressure crash scales like $S^{1/2}$. The increase of the core pressure after each crash also varies strongly with the resistive time. In essence, the rise and decay times of the pressure indicate behaviour similar to kink cycling in resistive MHD, with poorly separated time scales denoted by similar ramp and crash times.

It is emphasized that all the simulations in Fig. 8(a) resistive were performed with constant viscosity $\nu=5.0\times10^{-6}$, and $\chi_{\perp,0}=30\eta_0=3.10^{-6}-3.10^{-5}$. Comparing our results with the previous reduced MHD results revealed that no significant time scale discrepancy between the ramp and the crash characteristic times is observed in our simulations in $\eta\chi$MHD at the highest ratios of $\nu/\eta$ and $\nu/\chi_{\perp,0}$ in our study (50 and 1.67, respectively), contrary to Ref. 16. Increasing these ratios as in Ref. 16 is only of interest for very small tokamaks and is left open for future investigations.

### B. Sawtoothing regime

Now, we turn our attention to the sawtooth cycling regime, $\alpha\geq\alpha_2 S^{-3/5}$ (triangles and diamonds in Figs. 6 and 7). Fig. 2 shows pressure versus time at several radial locations in a simulation carried out with $\beta_p=0.22$, $S=2/3\times10^7$, and $\alpha=0.15$. Following a long quiescent ramp, a slowly growing precursor appears, causing the central pressure to slowly spiral out towards the $q=1$ surface. The precursor mode appears to quasi-saturate. Then, the profile relaxation accelerates, with the kinetic energy of the modes increasing by a factor of three in less than $500\tau_a$. This effect is due to the $\nabla\times\nabla_{||}p_e$ term in Faraday's equation.[12,20,21] Turning off the resistive term in Eq. (4) at the crash onset results in a slightly faster crash (about 5%). It appears, thus, that the resistivity does not affect the duration of the crash significantly.

Fig. 8(b) shows the central pressure evolution of several simulations carried out within the sawtooth cycling regime. For these cases, $S=1/3\times10^7-10^7$ and $\alpha=0.15$. (The effect of varying $\alpha$ on the crash time was already shown in Fig. 4.) With regard to Fig. 8(a), the crashes take place in a much shorter time frame, and the time scales of the ramp and crash are better separated. In effect, it appears that the rate of decrease in central pressure is equivalent during the deeply non-linear stage, while the appreciable difference in pressure just before the fast crash is due to a faster growing precursor for the cases with higher resistivity. The collapse of the hot pressure core is similar for all cases, varying between $300\tau_a$ and $900\tau_a$. Using the experimental values given in Sec. III A, this is equivalent to about 100–300 $\mu$s.

The dynamics observed at the crash onset can be interpreted as follows. We compare the diamagnetic frequencies with the rate of change of the kinetic energy of the $n=1$ mode, $\frac{1}{2}\frac{d}{dt}\ln K_{n=1}$. This quantity has units of frequency $\omega\tau_a$ and, during the linear phase, when the displacement is small, $\frac{1}{2}\frac{d}{dt}\ln K_{n=1}$ is equal to the linear growth rate. Starting in the linear phase, the precursor causes a radial displacement that decreases the available free energy. The rate of change of the energy, $\frac{1}{2}\frac{d}{dt}\ln K_{n=1}$, then decreases until it becomes

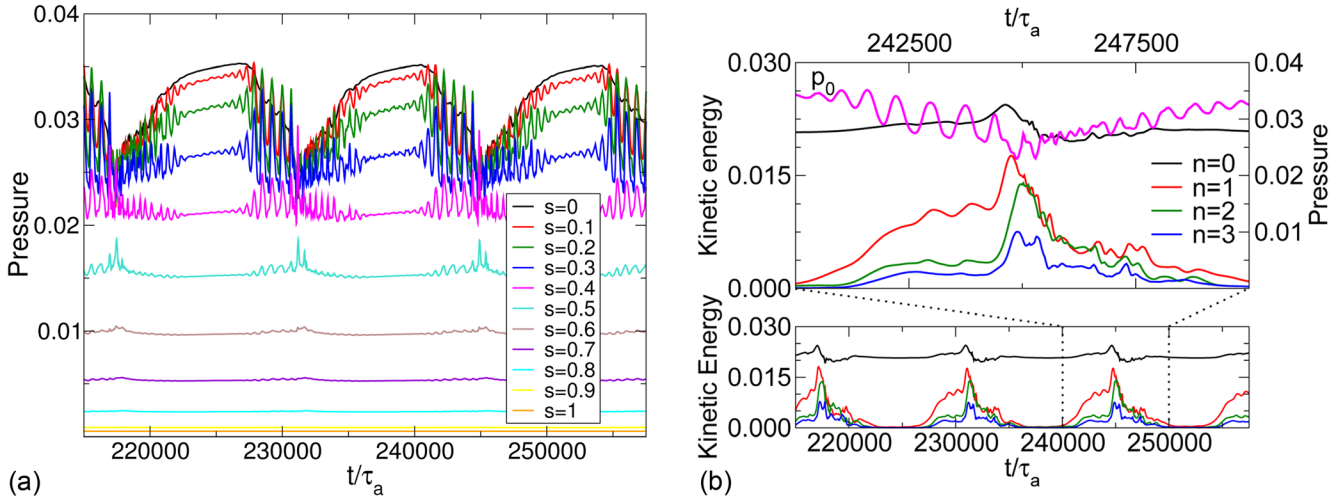


FIG. 10. (Color online) (a) Pressure versus time and (b) central pressure and kinetic energy of the $n=1, 2, 3$ modes during a kink crash (top) and kinetic energies of the $n=1, 2, 3$ modes for the same time interval as in (a) (bottom). Simulation has $S=1/3\times10^7$, $\beta_p=0.22$, and $\alpha=0.144$.

comparable to $\omega_{*e}$, which leads to even stronger diamagnetic damping (top and center panels of Fig. 9). Just before the pressure core collapse, the precursor saturates, triggering a fast release of kinetic energy. The ion diamagnetic frequency $\omega_{*i}$ is always very large compared to $\frac{1}{2}\frac{d}{dt}\ln K_{n=1}$. The electron diamagnetic frequency $\omega_{*e}^n$ enters the model through Faraday's law and is principally due to the density gradient.

The bottom panel of Fig. 9 shows the radius $r_{\text{peak}}$ and the horizontal position $x_{\text{peak}}=r_{\text{peak}}\cos(\theta_{\text{peak}})$ of the peak pressure on the poloidal plane defined by $\phi=0$, together with the location of the $q=1$ surface obtained when the precursor saturates. We measure $x_{\text{peak}}$ and $r_{\text{peak}}$ using our normalized radial coordinate $s$. At the crash onset, $r_{\text{peak}}\approx0.2$, which is consistent with the saturation of the precursor at a finite amplitude. During the crash, an increase of the poloidal precession frequency, i.e., the frequency of $x_{\text{peak}}$, and an acceleration of the displacement rate are observed respect to the precursor phase.

### C. Characterization of kink cycles near the $\alpha\approx\alpha_2 S^{-3/5}$ threshold

Finally, the cycle dynamics near the second diamagnetic threshold are examined.

In order to clarify the nature of the diamagnetic threshold between sustained kink cycles and the sawtooth cycles at $\alpha=\alpha_2 S^{-3/5}$ described in Sec. III, the ramp dynamics of a case slightly below the threshold for sawtoothing are described. A simulation with $\beta_p=0.22$, $S=1/3\times10^7$, and $\alpha=0.144$ is chosen. This case is displayed in Fig. 6 as belonging to the sustained kink cycling regime; the case with $\alpha=0.15$ yields sawtooth cycling.

The pressure evolution for several kink cycles is shown in Fig. 10(a) at different plasma radii. Note that the ramp stage of the internal kink cycle is never fully quiescent, with the pressure traces displaying oscillations due to a $m/n=1/1$ island. Moreover, the drop in the central pressure during each crash is rather slow, with $\tau_{\text{ramp}}/(\tau_{\text{precursor}}+\tau_{\text{crash}})\approx2$. The kinetic energy of the $n=0, 1, 2, 3$ modes is shown at the bottom of Fig. 10(b).

Upon closer examination, this case shows a two stage crash: a relatively long stage during which the modes appear to be quasi-saturated, resulting in the large pressure oscillations shown in Fig. 10(a); and a shorter period of accelerated reconnection. However, as shown in the bottom panel of Fig. 10(b), the growth rate acceleration appears to be triggered after almost all of the central pressure has been lost. Thus, in this case the diamagnetic drive due to the $\nabla\times\nabla_{||}p_e$ term does not shorten the crash. It appears that near the cyclic regime threshold two reconnection mechanisms compete, and a fast crash occurs only if the resistive instability (the precursor) is strongly stabilized.

## V. CONCLUSIONS

This paper attempts to quantify the scaling of some plasma conditions necessary to sustain kink cycles resembling sawtooth oscillations using a two-fluid MHD model (Eqs. (1)–(4)). The ramp dynamics of the internal kink were characterized using the quantities $S=1/\eta$ and $\alpha=(\omega_{ci}\tau_a)^{-1}$. A parameter scan in $S$ and $\alpha$ reveals a pattern of three regimes: (non-cyclic) stationary equilibria with $m/n=1/1$ helicity; kink cycles with resistive crashes roughly following Kadomtsev's predictions; and sawtooth-like kink cycles with fast crashes.

This sawtooth regime is characterized by quiescent ramps and two different instability timescales, which involve a slowly growing precursor mode and a phase of accelerated reconnection driven by diamagnetic effects. Using the present model, the fast crash onset appears to occur after strong diamagnetic stabilization of the precursor mode. The crash time appears not to be very sensitive to the resistivity.

The ramp dynamics at the diamagnetic threshold indicates that the triggering of the collisionless $m=1$ mode is insufficient for sustained sawtooth cycling. The second requirement for access into this regime appears to be the diamagnetic stabilization of a resistive $m=1$ kink mode in the deeply ideal MHD stable regime ($\lambda_H/\gamma_\eta\sim-1$). This resistive tearing-like mode must be strongly stabilized during the ramp phase and then again at the crash onset.

We note here that, in sawtooth regime observed in the simulations, the different timescales predicted by the analytical theory are reconciled with one another: the internal kink

is completely stabilized during the ramp; the precursor oscillations grow in the resistive timescale, and the crash takes place very rapidly.

While it is not possible to carry out simulations at realistic Lundquist numbers, the results of the parameter scan carried out indicate that diamagnetic effects alone may be sufficient to allow sustained sawtooth cycling in high temperature Ohmic tokamak plasmas. For instance, sawtooth cycles with fast crashes are recovered with $\alpha = 0.075$ at $S = 10^7$, while typically $\alpha \approx 0.08$ in Ohmic discharges in large tokamaks where $S \sim 10^8$. Due to the scaling of the stabilization threshold with resistivity, the sawtoothing regime is, in fact, more easily accessed at higher temperature. Consequently, in a two-fluid model, the sawtooth cycle at experimental parameters should consist of a quiescent ramp followed by a crash accelerated due to X-point reconnection.

It is noted that the MHD model for the reconnection used in the simulations is not complete, and that including electron inertia or polarization drift terms may affect the crash dynamics. The introduction of finite electron mass, in particular, could introduce a critical shear criterion for the crash onset, but would not alter the reconnection rate significantly.[11,12] The crash time would also be shorter if finite Larmor radius effects are taken into account.[14]

Finally, we emphasize that the present study was performed in $S - \alpha$ space with fixed $\beta_p$, below the marginal $\beta_p$ of the ideal internal kink by a factor $2/3$. The present work should be generalized to $\beta_p$ values characteristic of hot fusion tokamak plasmas, where the behavior of the internal kink dynamics described in the present work remains to be confirmed.

## ACKNOWLEDGMENTS

This work was carried out within the framework of the European Fusion Development Agreement and the French Research Federation for Fusion Studies (FR-FCM). It is supported by the European Communities under the contract of Association between EURATOM and CEA. The views and opinions expressed herein do not necessarily reflect those of the European Commission. The work of one of the authors (F.D.H.) was supported in part by the Swiss National Science Foundation.

[1]S. von Goeler, W. Stodiek, and N. Sauthoff, Phys. Rev. Lett. **33**, 1201 (1974).
[2]R. J. Hastie, Astrophys. Space Sci. Lib. **256**, 177 (1997).
[3]O. Sauter, E. Westerhof, M. L. Mayoral, B. Alper, P. A. Belo, R. J. Buttery, A. Gondhalekar, T. Hellsten, T. C. Hender, D. F. Howell, T. Johnson, P. Lamalle, M. J. Mantsinen, F. Milani, M. F. F. Nave, F. Nguyen, A. L. Pecquet, S. D. Pinches, S. Podda, and J. Rapp, Phys. Rev. Lett. **88**, 105001 (2002).
[4]T. C. Hender, J. C. Wesley, J. Bialek, A. Bondeson, A. H. Boozer, R. J. Buttery, A. Garofalo, T. P. Goodman, R. S. Granetz, Y. Gribov, O. Gruber, M. Gryaznevich, G. Giruzzi, S. Günter, N. Hayashi, P. Helander, C. C. Hegna, D. F. Howell, D. A. Humphreys, G. T. A. Huysmans, A. W. Hyatt, A. Isayama, S. C. Jardin, Y. Kawano, A. Kellman, C. Kessel, H. R. Koslowski, R. J. La Haye, E. Lazzaro, Y. Q. Liu, V. Lukash, J. Manickam, S. Medvedev, V. Mertens, S. V. Mirnov, Y. Nakamura, G. Navratil, M. Okabayashi, T. Ozeki, R. Paccagnella, G. Pautasso, F. Porcelli, V. D. Pustovitov, V. Riccardo, M. Sato, O. Sauter, M. J. Schaffer, M. Shimada, P. Sonato, E. J. Strait, M. Sugihara, M. Takechi, A. D. Turnbull, E. Westerhof, D. G. Whyte, R. Yoshino, H. Zohm, and the ITPA MHD and Disruption and Magnetic Control Topical Group, Nucl. Fusion **47**, S128 (2007).
[5]A. Fasoli, C. Gormenzano, H. Berk, B. Breizman, S. Briguglio, D. Darrow, N. Gorelenkov, W. Heidbrink, A. Jaun, S. Konovalov, R. Nazikian, J.-M. Noterdaeme, S. Sharapov, K. Shinohara, D. Testa, K. Tobita, Y. Todo, G. Vlad, and F. Zonca, Nucl. Fusion **47**, S264 (2007).
[6]M. N. Bussac, R. Pellat, D. Edery, and J. L. Soule, Phys. Rev. Lett. **35**, 1638 (1975).
[7]B. B. Kadomtsev, Sov. J. Plasma Phys. **1**, 389 (1975).
[8]G. Ara, B. Basu, B. Coppi, G. Laval, M. N. Rosenbluth, and B. V. Waddell, Ann. Phys. **112**, 443 (1978).
[9]R. E. Denton, J. F. Drake, and R. G. Kleva, Phys. Fluids **30**, 1448 (1987).
[10]F. L. Waelbroeck and R. D. Hazeltine, Phys. Fluids **31**, 1217 (1988).
[11]L. Zakharov and B. Rogers, Phys. Fluids B **4**, 3285 (1992).
[12]L. Zakharov, B. Rogers, and S. Migliuolo, Phys. Fluids B **5**, 2498 (1993).
[13]S. Migliuolo, Nucl. Fusion **33**, 1721 (1993).
[14]F. Porcelli, D. Boucher, and M. N. Rosenbluth, Plasma Phys. Controlled Nucl. Fusion Res. **38**, 2163 (1996).
[15]A. Y. Aydemir, J. C. Wiley, and D. W. Ross, Phys. Fluids B **1**, 774 (1989).
[16]G. Vlad and A. Bondeson, Nucl. Fusion **29**, 1139 (1989).
[17]H. Baty, J.-F. Luciani, and M. N. Bussac, Phys. Fluids B **5**, 1213 (1993).
[18]J. A. Wesson, Plasma Phys. Controlled Nucl. Fusion Res. **28**, 243 (1986).
[19]A. Y. Aydemir, Phys. Rev. Lett. **59**, 649 (1987).
[20]A. Y. Aydemir, Phys. Fluids B **4**, 3469 (1992).
[21]X. Wang and A. Bhattacharjee, Phys. Rev. Lett. **70**, 1627 (1993).
[22]D. Biskamp and J. F. Drake, Phys. Rev. Lett. **73**, 971 (1994).
[23]F. D. Halpern, D. Leblond, H. Lütjens, and J.-F. Luciani, Plasma Phys. Controlled Nucl. Fusion Res. **53**, 015011 (2011).
[24]H. Lütjens and J.-F. Luciani, J. Comput. Phys. **229**, 8130 (2010).
[25]S. I. Bragniskii, *Transport Processes in a Plasma*, Reviews of Plasma Physics, edited by M. A. Leontovich (Consultants Bureau, New York, 1965), Vol. 1, p. 205.
[26]R. Hazeltine and J. D. Meiss, *Plasma Confinement*, The Advanced Book Program (Addison-Wesley, Redwood City, CA, 1992), p. 228.
[27]H. Lütjens and J.-F. Luciani, J. Comput. Phys. **227**, 6944 (2008).
[28]H. Lütjens, A. Bondeson, and O. Sauter, Comput. Phys. Commun. **97**, 219 (1996).
[29]B. Rogers and L. Zakharov, Phys. Plasmas **3**, 2411 (1996).